

NRC Publications Archive Archives des publications du CNRC

Designing majorana quasiparticles in InAsP quantum dots in InP nanowires with variational quantum eigenvalue solver

Mohseni, Mahan; Cunha, Iann; Miravet, Daniel; Wania Rodrigues, Alina; Allami, Hassan; Assi, Ibsal; Korkusinski, Marek; Hawrylak, Pawel

This publication could be one of several versions: author's original, accepted manuscript or the publisher's version. / La version de cette publication peut être l'une des suivantes : la version prépublication de l'auteur, la version acceptée du manuscrit ou la version de l'éditeur.

For the publisher's version, please access the DOI link below. / Pour consulter la version de l'éditeur, utilisez le lien DOI ci-dessous.

Publisher's version / Version de l'éditeur:

<https://doi.org/10.1002/pssb.202400552>

physica status solidi (b): basic solid state physics (PSSB), 2025-03-09

NRC Publications Archive Record / Notice des Archives des publications du CNRC :

<https://nrc-publications.canada.ca/eng/view/object/?id=05f0a1af-c6ad-4925-b75a-693d71146909>

<https://publications-cnrc.canada.ca/fra/voir/objet/?id=05f0a1af-c6ad-4925-b75a-693d71146909>

Access and use of this website and the material on it are subject to the Terms and Conditions set forth at

<https://nrc-publications.canada.ca/eng/copyright>

READ THESE TERMS AND CONDITIONS CAREFULLY BEFORE USING THIS WEBSITE.

L'accès à ce site Web et l'utilisation de son contenu sont assujettis aux conditions présentées dans le site

<https://publications-cnrc.canada.ca/fra/droits>

LISEZ CES CONDITIONS ATTENTIVEMENT AVANT D'UTILISER CE SITE WEB.

Questions? Contact the NRC Publications Archive team at

PublicationsArchive-ArchivesPublications@nrc-cnrc.gc.ca. If you wish to email the authors directly, please see the first page of the publication for their contact information.

Vous avez des questions? Nous pouvons vous aider. Pour communiquer directement avec un auteur, consultez la première page de la revue dans laquelle son article a été publié afin de trouver ses coordonnées. Si vous n'arrivez pas à les repérer, communiquez avec nous à PublicationsArchive-ArchivesPublications@nrc-cnrc.gc.ca.

Designing Majorana Quasiparticles in InAsP Quantum Dots in InP Nanowires with Variational Quantum Eigenvalue Solver

Mahan Mohseni,* Iann Cunha, Daniel Miravet, Alina Wania Rodrigues, Hassan Allami, Ibsal Assi, Marek Korkusinski, and Pawel Hawrylak


This work presents steps toward the design of Majorana zero modes (MZM) in InAsP quantum dots embedded in an InP semiconducting nanowire in contact with a p-type superconductor described by the Kitaev Hamiltonian. The single-particle spectrum is obtained from million atom atomistic calculations with QNANO and many-electron spectra using exact diagonalization and the hybrid variational quantum eigensolver (VQE) method. A variational ansatz is constructed to capture the ground state of the system by utilizing a generalized form of the analytical solution for a particular set of parameters. By systematically deviating from the analytically solvable regime while maintaining the system in the topological phase, the effectiveness of the variational function in reproducing the correct ground state and topological properties of the system is evaluated. This is done through a quantum algorithm for a many-body state containing MZM. The results are compared with exact solution in topological phase and demonstrate the capability of VQE, along with classical simulations, to accurately model the many-body spectra in topologically nontrivial state.

1. Introduction

We explore here an array of InAsP semiconductor quantum dots (QDs) in InP nanowire as a host for Majorana quasiparticles

M. Mohseni, I. Cunha, D. Miravet, A. Wania Rodrigues, H. Allami, I. Assi, P. Hawrylak
Department of Physics
University of Ottawa
Ottawa K1N 6N5, Canada
E-mail: mghaf073@uottawa.ca

M. Korkusinski
Quantum and Nanotechnology Research Center
National Research Council
Ottawa K1A 0R6, Canada

 The ORCID identification number(s) for the author(s) of this article can be found under <https://doi.org/10.1002/pssb.202400552>.

© 2025 The Author(s). physica status solidi (b) basic solid state physics published by Wiley-VCH GmbH. This is an open access article under the terms of the Creative Commons Attribution-NonCommercial License, which permits use, distribution and reproduction in any medium, provided the original work is properly cited and is not used for commercial purposes.

DOI: 10.1002/pssb.202400552

for topological quantum computation. Topological quantum computation^[1–5] is a robust framework for realizing fault-tolerant quantum computing,^[6–9] which aims to perform computations reliably despite the presence of noise and errors.^[3,10,11]

A promising candidate for implementing this protection is Majorana zero modes (MZM).^[12] MZMs are quasiparticles that arise in topological phases of matter, particularly in systems that combine strong spin-orbit coupling with superconductivity.^[13] Their non-abelian statistics enable fault-tolerant quantum gates through the process of braiding-exchanging the positions of MZM modes. Unlike conventional qubits, which are vulnerable to local noises, the information stored in MZMs is distributed non-locally, making it protected from decoherence.

A candidate to host MZMs is the 1D chain of InAs QDs in InP nanowire^[14,15]

containing spinless fermions with nearest-neighbor hopping and p-wave superconducting pairing, namely the Kitaev chain.^[9,16,17] In its topological phase (TP), the Kitaev chain hosts MZMs at its ends, where the fermionic excitations split into two spatially separated Majorana particles, each localized at opposite ends of the chain.^[9,16,17]

We describe here one electron properties of the nanowire using QNANO code^[18,19] and many-body properties using exact diagonalization (ED) on a classical computer^[17] and VQE on a quantum computer.

While ED method provides exact solutions, its applicability is limited by the exponential growth of the Hilbert space. For instance, for chain with $N = 25$ QDs the Hamiltonian matrix has the dimension 2^{25} . Hence ED is limited to relatively small systems. In this study, we try to find an estimate of the ground state energy of the Kitaev Hamiltonian on a quantum computer,^[20,21] using the VQE method. We use analytical and numerical ED to compute the full energy spectrum^[17] and then implement VQE to compute even and odd ground states by constructing a quantum circuit guided by the analytical solution.^[17] By comparing the VQE results with those from ED, we demonstrate that VQE provides an accurate estimate of the ground state energy for large systems.

2. Semiconductor Nanowire as Kitaev Chain

The Kitaev chain considered in this work is implemented in a hexagonal InP nanowire with an array of embedded InAsP QDs in the proximity of a p-wave superconductor and in the presence of applied external magnetic field.^[17,22–27] The QD nanowire is schematically shown in **Figure 1**. We performed microscopic calculations of single-particle spectrum using QNANO code^[18,19] for electron in one and two InAsP QDs embedded within an InP nanowire to determine the energy of the lowest conduction band states in a QD and interdot tunneling t in the InAsP QD array. QNANO calculations are based on ab initio-based tight-binding model, where the QD nanowire is created by first establishing an InP matrix and defining a hexagonal nanowire within it, as illustrated in **Figure 2a,b**. Next, random P atoms are replaced with As atoms at a concentration of 20%. **Figure 2c** displays the energy levels of the electron in the conduction band of a double QD, highlighting the characteristics s, p, and d shells of an isolated QD, which are split due to the tunneling between the two QDs. Despite the random distribution of As atoms, the spectrum reveals a well-defined s shell followed by two states of the p shell.^[15,28,29]

By applying a strong magnetic field along the nanowire, we can isolate the low energy spin component and treat those electrons as spinless. In this context, for p-wave superconductor the non-interactive Kitaev Hamiltonian^[16,17] is given as

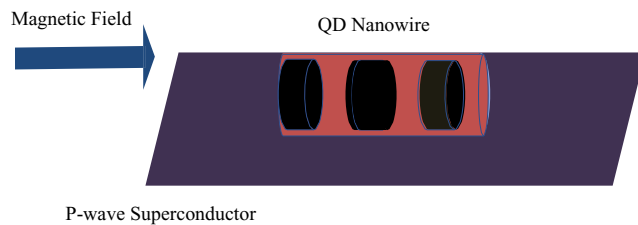


Figure 1. Schematic visualization of the chain of QDs (in black) in a nanowire (red). The QD nanowire is placed on top of a p-wave superconductor (violet). The external magnetic field (blue) is along the nanowire.

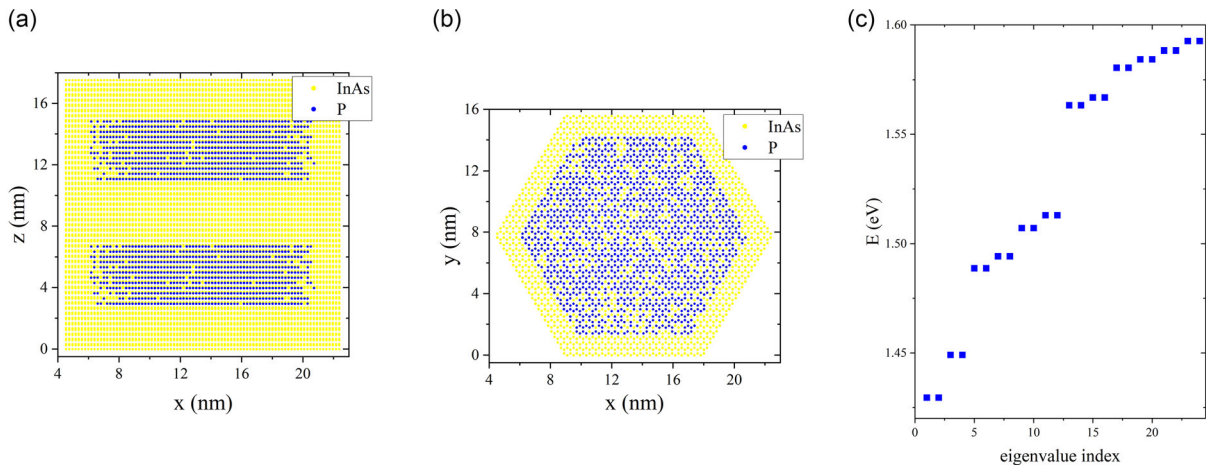


Figure 2. a) Side cross sections of double QDs nanowire. b) Top cross sections of double QDs nanowire. c) Single-particle spectrum of conduction band electron in a double quantum dot. The splitting of two degenerate s-levels by tunneling is visible. The degeneracy is due to spin.

$$\hat{H} = t \sum_{i=1}^{N-1} (c_{i+1}^\dagger c_i + h.c.) + \Delta \sum_{i=1}^{N-1} (c_{i+1}^\dagger c_i^\dagger + h.c.) - \mu \sum_{i=1}^N c_i^\dagger c_i \quad (1)$$

where c_i^\dagger (c_i) is the fermionic creation (annihilation) operator of an electron in dot i , t is tunneling matrix element between adjacent conduction s-levels, Δ is the pairing energy for two electrons on adjacent conduction levels, and μ is the chemical potential measured from the conduction energy level. This Hamiltonian is valid as long as the t and Δ are small compared with energy levels of s and p-shell.

2.1. Exact Diagonalization and Many-Body Spectrum of Kitaev Chain

The many-body spectrum of the Kitaev Hamiltonian was obtained earlier in ref. [17] and we summarize it here for completeness. The ED method involves expanding the wave function in terms of all configurations for even and odd number of electrons, constructing the full Hamiltonian matrix in the space of configurations and diagonalizing it to obtain its eigenvalues and eigenvectors, providing exact solutions for finite-sized systems. In case of N spinless orbitals, there are 2^N configurations constructed as

$$|\alpha_1 \dots \alpha_N\rangle = \prod_{i=1}^N (c_i^\dagger)^{\alpha_i} |0\rangle \quad (2)$$

where $|0\rangle$ is the vacuum of electrons, $\alpha_i = 1$ or 0 , corresponds to having 1 or 0 electron in orbital i .

The pairing term in the Kitaev Hamiltonian changes the particle number but conserves parity, hence the eigenstates are linear combinations of electronic configurations with different electron numbers but given parity

$$|\psi^\nu\rangle = \sum_{M, p_M} C_{M, p_M}^\nu |M, p_M\rangle \quad (3)$$

where we are populating N sites with $M = 0, 1, \dots, N$ electrons, and for a given number of electrons M we generate electron configurations p_M . In order to obtain the coefficients C_{M, p_M}^ν , we apply

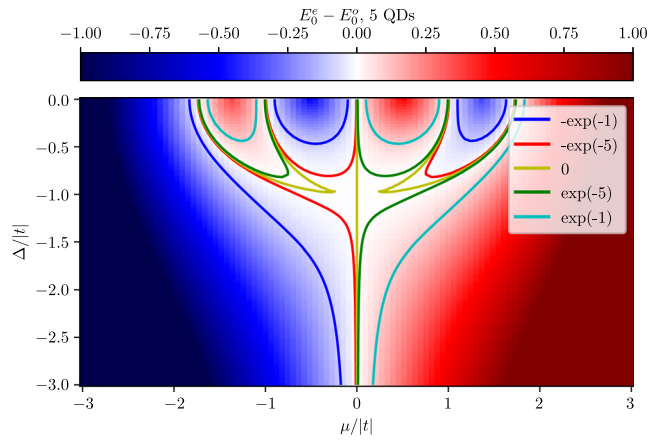


Figure 3. Ground state energy difference of the even and odd subspaces for a chain of 5 QDs, by using ED, with $t = -1$. The contours show the boundaries between the trivial and the TP with various precision, based on the size of the chain.

the Hamiltonian to this state, and by using the orthogonality of the configurations we obtain the eigenvalue equation

$$\sum_{p_M, M} \langle q_{M'}, M | \hat{H} | p_M, M \rangle C_{M, p_M}^\nu = E^\nu C_{M, p_M}^\nu \quad (4)$$

Since the Kitaev Hamiltonian in Equation (1) only changes particle number in pairs, the matrix element $\langle q_{M'}, M | \hat{H} | p_M, M \rangle$ is non-zero only if M and M' have the same parity, that is, if they are both even or odd. This parity symmetry allows us to break the Hilbert space into two decoupled subspaces of even and odd configurations.

Results of the ED for $N = 5$ QDs are shown in **Figure 3**, where the energy difference between the even and odd electron numbers is plotted.^[17] The system is in TP as long as the difference is zero. The MZMs appear when the system is in the TP, where the ground state is doubly degenerate, with one state corresponding to the even and the other one corresponding to the odd subspace. The TP is centered at $t = \Delta$ and $\mu = 0$,^[4,17] for which analytical solution exists. It can be shown that as long as $2|t| > \mu$, the system remains in the TP,^[16,30] as seen in Figure 3. The numerical ED can be carried out for small chains for any set of parameters, but alternative methods have to be applied for large systems.

We now turn to the main objective of this work, that is, the application of VQE method and quantum computer to determining the ground states for even/odd number of electrons and presence or absence of the TP with MZMs.

3. Variational Quantum Eigensolver for a Kitaev Chain

The VQE is a hybrid method that aims to estimate the ground state energy of a given Hamiltonian through a quantum-classical computational approach.^[31,32] The benefit of quantum comes from the capacity to manage and manipulate the variational states as quantum circuits.^[33,34] The variational state is generated by a unitary operation (quantum circuit) acting on an initial state. By using a classical optimizer to fine-tune the variational

parameters of the quantum circuit, VQE minimizes the energy for large systems.^[35–37]

The first step in the VQE workflow is to express the Hamiltonian \hat{H} in terms of Pauli operators, through the Jordan–Wigner (JW) transformation. A quantum circuit with adjustable gates, parameterized by parameters θ , is then applied to generate the quantum state $|\psi(\theta)\rangle$, where θ represents a set of parameters used in a quantum circuit, allowing the Hamiltonian written in Pauli operators to act on the state $|\psi(\theta)\rangle$. The expectation value of the energy is measured using the quantum computer as follows:

$$E(\theta) = \langle \psi(\theta) | \hat{H} | \psi(\theta) \rangle \quad (5)$$

The measured energy $E(\theta)$ is fed into the classical optimizer, which adjusts the parameters θ to minimize the energy. This process is iterated, repeating the quantum circuit execution and the measurement, with the optimizer refining θ until the minimum energy is found. Ultimately, the optimized parameters correspond to the approximate ground state of the Hamiltonian, providing a solution to the problem.

3.1. Jordan–Wigner (JW) Transformation–Kitaev Chain on a Quantum Computer

The JW transformation maps fermionic operators into spin operators represented by the Pauli matrices, and spin operators into qubits of a quantum computer.^[38,39]

The JW transformation for spinless fermions is defined as

$$c_j^\dagger = e^{-i\Phi_j} S_j^+ \quad (6a)$$

$$c_j = S_j^- e^{i\Phi_j} \quad (6b)$$

where $S_j^\pm = S_j^\pm \pm iS_j^y$ are the rising and lowering spin operators for site j , and $\vec{S} = \frac{1}{2}\vec{\sigma}$ are the spin- $\frac{1}{2}$ operators. The phase factor Φ_j can be express as

$$\Phi_j = \pi \sum_{m=1}^{j-1} \left(\frac{1}{2} + S_m^z \right) \quad (7)$$

which introduces non-locality in the mapping, ensuring that the fermionic operators obey the correct anti-commutation relations. Therefore, by using the exponential term as $e^{\pm i\Phi_j} = \prod_{m=1}^{j-1} (-2S_m^z)$, as previously demonstrated in refs. [40,41], the fermionic products transform as

$$c_i^\dagger c_i = S_i^+ S_i^- \quad (8)$$

$$c_{i+1}^\dagger c_i = S_{i+1}^+ S_i^- \quad (9)$$

$$c_{i+1}^\dagger c_i^\dagger = -S_{i+1}^+ S_i^+ \quad (10)$$

After this transformation, the fermionic states $|0\rangle$ and $|1\rangle$, representing the vacant or occupied site, correspond to spin-down $|\downarrow\rangle$ and spin-up $|\uparrow\rangle$, respectively. This establishes a direct correspondence between the fermionic and spin bases. Finally, the Hamiltonian in Equation (1) is transformed into spin Hamiltonian

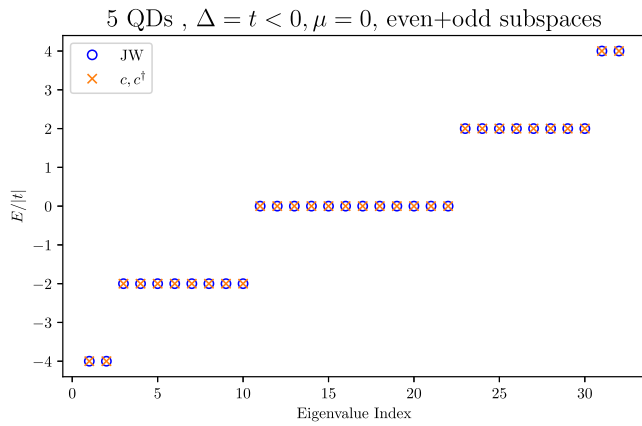


Figure 4. Energy spectra matching of the fermionic and spin Hamiltonian in the analytical solution case. The even (odd) eigenvalue indices correspond to the even (odd) subspace eigenvalues.

$$\hat{H} = -\frac{\mu N}{2} - \mu \sum_{i=1}^N S_i^z + 2 \sum_{i=1}^{N-1} [(t + \Delta) S_{i+1}^y S_i^y + (t - \Delta) S_{i+1}^x S_i^x] \quad (11)$$

expressed in terms of the spin operators S_i^x , S_i^y , and S_i^z . By comparison with the XY model,

$$\hat{H} = -h \sum_{i=1}^N S_i^z + \sum_{i=1}^{N-1} [J_y S_{i+1}^y S_i^y + J_x S_{i+1}^x S_i^x] \quad (12)$$

we see that the Kitaev Hamiltonian in spin representation is essentially an XY model, with μ acting as the external magnetic field along the z -direction, J_x as the $t - \Delta$ term, and J_y as the $t + \Delta$ term.

In **Figure 4**, we show results using ED of the fermionic Kitaev Hamiltonian and spin Kitaev Hamiltonian obtained through JW transformation. This figure shows that the spectra are identical and we can proceed to implementing VQE on a quantum computer.

3.2. Quantum Circuit and Variational Wave Function

We utilize four ansätze (quantum circuits) throughout the variational calculation, namely even, odd, efficient SU(2), and Hamiltonian variational ansatz (HVA).^[42,43] Inspired by the fact that in the TP, the ground state of even (odd) subspace has equal contribution of all even (odd) configurations, we construct the even (odd) ansatz based on this feature, that is, we consider all configurations in the subspace, and assign variational parameters to them.

The efficient SU(2) consists of layers of single-qubit operations spanned by the SU(2) group and CX entanglements. HVA is directly built from the Hamiltonian (see Appendix A). As an illustration, we look at the even ansatz for three qubits in **Figure 5**. This ansatz essentially creates all the even configurations using the R_y and CNOT operations, and assigns variational parameters to each configuration.

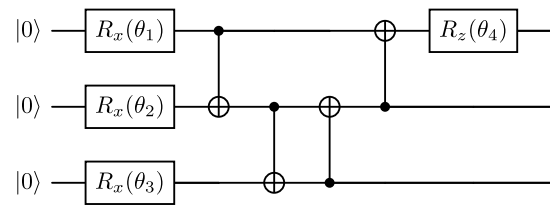


Figure 5. The quantum circuit for the even ansatz with three qubits. The gates are applied as: a set of R_x gates applied to each qubit. Then, CNOT gates are applied in a forward direction between consecutive qubits. After that, reverse CNOT gates are applied in reverse order. Finally, a single R_z gate is applied only to the first qubit (qubit 0).

$$|\psi(\theta)\rangle_{\text{even}} = R_z^{(0)}(\theta_{N+1}) \prod_{j=1}^{N-1} \text{CX}^{(j+1,j)} \prod_{j=1}^{N-1} \text{CX}^{(N-j,j-N+1)} \times \prod_{j=1}^N R_x^{(j)}(\theta_j) |\psi_0\rangle \quad (13)$$

4. Results of VQE

4.1. Comparison of Quantum Circuits for Variational Ansätze

In order to make a transparent comparison between the performance of different ansätze, we examine the loss function behavior, which in this case is the ground state energy.

As shown in **Figure 6**, although HVA is the fastest to reach convergence, the even, SU2, and odd ansätze have smaller error, especially in the non-analytical solution case. Each ansatz stops at a particular optimization step once the classical optimizer decides it has converged. For each ansatz, the best number of parameters is used from studying the relative error behavior for various number of parameters, discussed in Appendix B.

In **Figure 6a**, the performance of each ansatz is shown in the analytical solution regime. The ground state energy for even, odd, and SU2 ansätze is closer to the exact ground state energy, compared to HVA.

In **Figure 6b**, although there is no analytical solution for the choice of parameters, the system still lies in the TP. The exact ground state energy is obtained using numerical ED. The performance of each ansatz is displayed for their best number of parameters in Appendix B. Although the optimization process is more challenging in this case, the ground state energy for even, odd, and SU2 ansätze indicate reliable performance, while HVA stops in the early optimization steps, with a significant error.

This reveals a clear distinction in the performance of the different ansätze when comparing the relative error. For the even, odd, and SU2 ansätze, convergence to the actual ground state energy is achieved with an insignificant relative error. In contrast, despite the fast convergence, the HVA ansatz shows a higher relative error, specifically in the non-analytical case.

4.2. Error Sensitivity within the Topological Phase

Having demonstrated the convergence of the variational functions, we now explore the sensitivity of the approximated ground

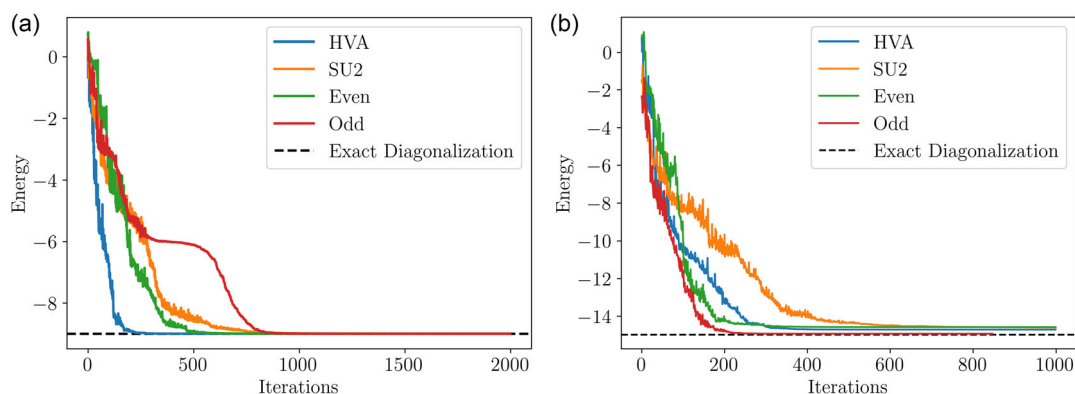


Figure 6. Ground state energy as a function of optimization steps for four ansätze: Even, odd, SU2, and HVA, for a chain of 10 QDs. The comparison highlights the convergence pattern and efficiency of each ansatz in minimizing the ground state energy. a) corresponds to the analytical case with $\Delta = t$ and $\mu = 0$, while b) represents a case outside the analytical regime but still within the topological phase, with $\Delta = 2t$ and $\mu = -0.2t$. The optimal number of parameters is used in both cases.

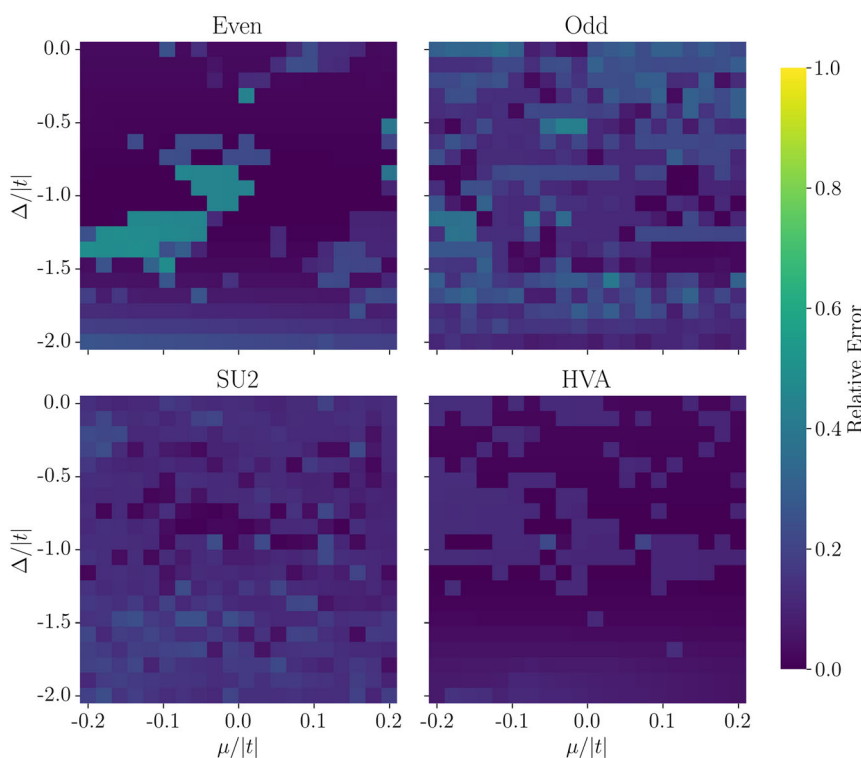


Figure 7. Evolution of the relative error in the parameter space for various ansätze, for a chain of 10 QDs. The choice of the parameters $\Delta/|t|$ and $\mu/|t|$ is such that the system remains in the TP. The dark regions indicate areas of lower relative error, with the analytical solution located at the center of the plots.

state energy as the parameters scale up in the TP. To do so, we analyze the relative error for each ansatz while we tune the parameters within the TP in the parameter space.

Figure 7 visualizes the performance of each variational ansatz by displaying the relative error as a function of $\Delta/|t|$ and $\mu/|t|$. The special case where the analytical solution case is at the center of each figure. Except for the HVA case, as the parameters deviate

from this case, the relative error increases. Each ansatz exhibits a unique error profile, highlighting differences in how well they adapt to variations in the Hamiltonian. However, the even, odd, and SU2 ansätze outperform HVA. This disparity of performance highlights the suitability of the even, odd, and SU2 ansätze for accurately modeling the system compared to more complex alternatives like the HVA.

5. Conclusion

In summary, we presented steps toward designing Majorana Quasiparticles in InAsP QD in InP Nanowires on p-wave superconductor with QNANO and variational quantum eigenvalue (VQE) solver on a quantum computer. We used VQE approach to estimate the ground state energy of the semiconducting QD nanowire in the proximity of a p-wave superconductor, in the presence of applied external magnetic field, described by the Kitaev chain. We used QNANO to obtain single-particle spectra and showed that by constructing the optimal quantum circuit for variational wave function from the analytical solution of the system, we can determine the odd and even ground state energy and hence determine the topological phase of the Kitaev chain. Moreover, the topological features of the wave function remain preserved, thus enabling the system to host MZMs. Future work will focus on simulating spinfull fermions in semiconducting InAs quantum dots in InP nanowires with Rashba spin-orbit coupling on s-type superconductors.

Appendix A: Ansatz Construction

As mentioned before, we use four different ansätze, namely even, odd, efficient SU(2), and HVA. The even ansatz is already described in Figure 5. The odd ansatz is a variational function that contains all the odd subspace configurations (Figure A1).

$$|\psi(\theta)\rangle_{\text{odd}} = \prod_{j=1}^N R_Z^{(j)}(\theta_{N+j}) \prod_{j=1}^{N-1} CX^{(j+1,j)} \prod_{j=1}^{N-1} CX^{(N-jj-N+1)} \times \prod_{j=1}^N R_X^{(j)}(\theta_j) |\psi_0\rangle \quad (\text{A1})$$

The efficient SU(2) (Figure A2 and A3), namely from the special unitary group, consists of layers of single-qubit rotations (R_Y and R_Z gates) and entangling gates (CNOT) arranged to capture correlations between qubits. By applying these operations across multiple layers, the ansatz can approximate the ground state of complex quantum systems with fewer resources than more traditional methods.

$$|\psi(\theta)_{\text{SU2}}\rangle = \prod_{j=1}^N R_Y^{(j)}(\theta_{2j-1}) R_Z^{(j)}(\theta_{2j}) \prod_{j=1}^{N-1} CX^{(j+1,j)} \times \prod_{j=1}^N R_Y^{(j)}(\theta_{2N+2j-1}) R_Z^{(j)}(\theta_{2N+2j}) |\psi_0\rangle \quad (\text{A2})$$

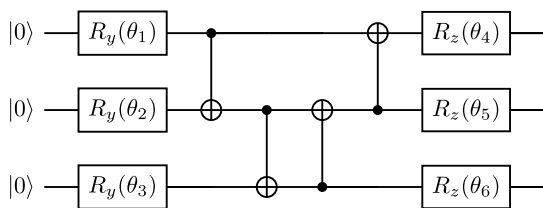


Figure A1. The quantum circuit for the odd ansatz with three qubits. The gates are applied as: a set of R_Y gates applied to each qubit. Then, CNOT gates are applied in a forward direction between consecutive qubits. After that, revers CNOT gates applied in the reverse order. Finally, a set of R_Z gate is applied to each qubit.

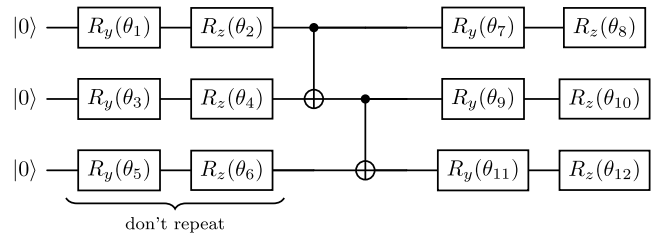


Figure A2. Quantum circuit of the SU2 ansatz with three qubits and one layer of linear entanglement.

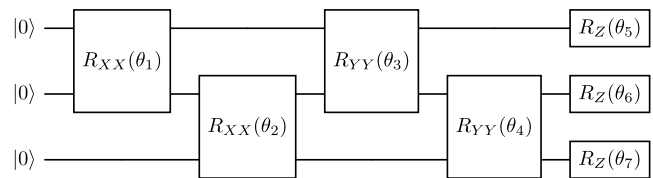


Figure A3. The quantum circuit for the HVA with three qubits.

The last ansatz we consider is the HVA. To construct it, we decompose the Kitaev Hamiltonian, express in Equation (12), in to a sum of non-commuting terms

$$\hat{H} = \frac{t - |\Delta|}{2} \sum_{j=1}^{N-1} (S_{j+1}^x S_j^x) + \frac{t + |\Delta|}{2} \sum_{j=1}^{N-1} (S_{j+1}^y S_j^y) - \frac{\mu}{2} \sum_{j=1}^N S_j^z - \frac{\mu N}{2} \quad (\text{A3})$$

For a decompose Hamiltonian $\hat{H} = \sum_{i=1}^q c_j \hat{H}^{(j)}$, where $\{c_j\}$ are the real coefficient, each term in the Hamiltonian corresponds to a unitary variational operator $\hat{U}_j = \exp(-i\theta_j \hat{H}^{(j)})$, associated with a variational parameters θ_j , that contributes to the overall HVA circuit. Then, the Kitaev HVA is constructed as

$$\hat{U}(\theta) = \prod_{k=1}^R \left[\prod_{j=1}^{N-1} \exp\{-i\theta_j^x (S_{j+1}^x S_j^x)\} \times \prod_{j=1}^{N-1} \exp\{-i\theta_j^y (S_{j+1}^y S_j^y)\} \prod_{j=1}^N \exp\{-i\theta_j^z S_j^z\} \right] \quad (\text{A4})$$

Another step it to apply a second-order Trotter–Suzuki decomposition to implement each exponential operator \hat{U}_j . This method approximates the time evolution operator by applying each term in sequence, alternating the order of application to reduce errors, from what is already established.^[43]

Appendix B: Ansatz Optimization

To improve the performance of each ansatz, we optimize them based on the number of layers and how we can minimize the relative error. To do so, we plot the relative error versus the number of layers (parameters) of each ansatz. For a given number of layers, we take the minimum energy of 10 initial runs. The entire optimization is done using the COBYLA optimizer available in the Qiskit package, and 30 000 shots.

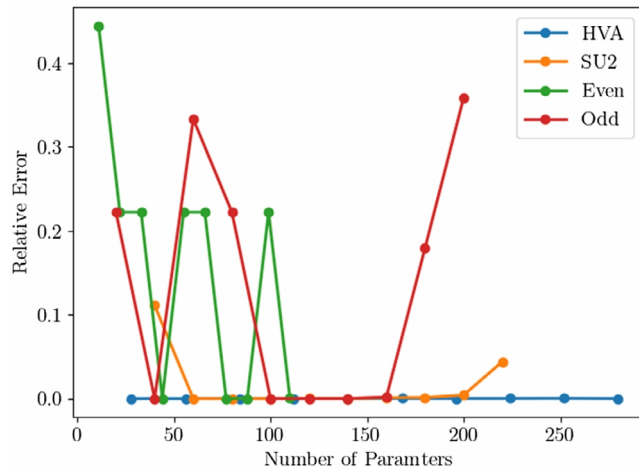


Figure A4. Relative error as a function of the number of parameters for different ansätze in the analytical solution regime, $\Delta = t$ and $\mu = 0$, for a chain of 10 QDs. The maximum number of layers is 10.

In **Figure A4**, each ansatz is evaluated across varying numbers of layers, with the number of layers ranging from 1 to 10. The relative error is plotted on the y -axis

$$\text{Error} = \left| 1 - \frac{E_{\text{VQE}}}{E_{\text{ED}}} \right| \quad (\text{A5})$$

while the number of parameters on the x -axis, allowing for a direct comparison of how the error changes with increasing the number of layers for each ansatz. The number of parameters per layer for the even, odd, SU2, and HVA ansätze are 11, 20, 40, and 28, respectively.

Acknowledgements

P.H., M.M., D.M., I.A., I.C., and A.W.R. were supported by the AQC-004 project of the Applied Quantum Computing Program at the National Research Council of Canada, NSERC Discovery grant no. RGPIN 2019-05714, NSERC Alliance Quantum grant no. ALLRP/578466-2022, the QSP-078 project of the Quantum Sensors Program at the National Research Council of Canada, University of Ottawa Research Chair in Quantum Theory of Materials, Nanostructures, and Devices, and Digital Research Alliance Canada with computing resources.

Conflict of Interest

The authors declare no conflict of interest.

Data Availability Statement

The data that support the findings of this study are available from the corresponding author upon reasonable request.

Keywords

Majorana zero mode, quantum computation, semiconductor nanowires, semiconductor quantum dots, topological superconductor, variational quantum eigensolver

Received: October 15, 2024

Published online:

- [1] M. Freedman, A. Kitaev, M. Larsen, Z. Wang, *Bull. Am. Math. Soc.* **2003**, *40*, 31.
- [2] S. Das Sarma, M. Freedman, C. Nayak, *Phys. Today* **2006**, *59*, 2.
- [3] P. Marra, *J. Appl. Phys.* **2022**, *132*, 23.
- [4] S. D. Sarma, M. Freedman, C. Nayak, *npj Quantum Inf.* **2015**, *1*, 1.
- [5] B. Field, T. Simula, *Quantum Sci. Technol.* **2018**, *3*, 045004.
- [6] D. Gottesman, *Phys. Rev. A* **1998**, *57*, 127.
- [7] J. Preskill, *Introduction to Quantum Computation and Information*, World Scientific **1998**, pp. 213–269.
- [8] P. W. Shor, in *Proc. of 37th Conf. on Foundations of Computer Science*, IEEE, Burlington, VT, USA **1996**, pp. 56–65.
- [9] A. Y. Kitaev, *Ann. Phys.* **2003**, *303*, 2.
- [10] S. L. Braunstein, H.-K. Lo, *Scalable Quantum Computers: Paving the Way to Realization*, Wiley-VCH **2001**.
- [11] J. I. Cirac, P. Zoller, *Nature* **2000**, *404*, 579.
- [12] Y. Kim, J. Cano, C. Nayak, *Phys. Rev. B: Condens. Matter Mater. Phys.* **2012**, *86*, 235429.
- [13] K. Flensberg, F. von Oppen, A. Stern, *Nat. Rev. Mater.* **2021**, *6*, 944.
- [14] Z.-X. Koong, G. Ballesteros-Garcia, R. Proux, D. Dalacu, P. J. Poole, B. D. Gerardot, *Phys. Rev. Appl.* **2020**, *14*, 034011.
- [15] P. Laferriere, E. Yeung, M. Korkusinski, P. J. Poole, R. L. Williams, D. Dalacu, J. Manalo, M. Cygorek, A. Altintas, P. Hawrylak, *Appl. Phys. Lett.* **2021**, *118*, 16.
- [16] A. Y. Kitaev, *Phys. Usp.* **2001**, *44*, 131.
- [17] M. Mohseni, H. Allami, D. Miravet, D. J. Gayowsky, M. Korkusinski, P. Hawrylak, *Nanomaterials* **2023**, *13*, 2293.
- [18] M. Zieliński, M. Korkusiński, P. Hawrylak, *Phys. Rev. B: Condens. Matter Mater. Phys.* **2010**, *81*, 085301.
- [19] M. Cygorek, M. Korkusinski, P. Hawrylak, *Phys. Rev. B* **2020**, *101*, 075307.
- [20] M. Thakurathi, K. Sengupta, D. Sen, *Phys. Rev. B* **2014**, *89*, 235434.
- [21] L. Chen, W. LiMing, J.-H. Huang, C. Yin, Z.-Y. Xue, *Phys. Rev. A* **2014**, *90*, 012323.
- [22] E. Talantsev, K. Iida, T. Ohmura, T. Matsumoto, W. Crump, N. Strickland, S. Wimbush, H. Ikuta, *Sci. Rep.* **2019**, *9*, 14245.
- [23] W.-S. Wang, C.-C. Zhang, F.-C. Zhang, Q.-H. Wang, *Phys. Rev. Lett.* **2019**, *122*, 027002.
- [24] N. F. Yuan, K. F. Mak, K. Law, *Phys. Rev. Lett.* **2014**, *113*, 097001.
- [25] P. Frigeri, D. Agterberg, A. Koga, M. Sgrist, *Phys. Rev. Lett.* **2004**, *92*, 097001.
- [26] F. Hardy, A. Huxley, *Phys. Rev. Lett.* **2005**, *94*, 247006.
- [27] K. Ishida, H. Mukuda, Y. Kitaoka, K. Asayama, Z. Mao, Y. Mori, Y. Maeno, *Nature* **1998**, *396*, 658.
- [28] J. Manalo, D. Miravet, P. Hawrylak, *Phys. Rev. B* **2024**, *109*, 085112.
- [29] J. Manalo, M. Cygorek, A. Altintas, P. Hawrylak, *Phys. Rev. B* **2021**, *104*, 125402.
- [30] M. Leijnse, K. Flensberg, *Semicond. Sci. Technol.* **2012**, *27*, 124003.
- [31] D. A. Fedorov, B. Peng, N. Govind, Y. Alexeev, *Mater. Theory* **2022**, *6*, 2.
- [32] J. Tilly, H. Chen, S. Cao, D. Picozzi, K. Setia, Y. Li, E. Grant, L. Wossnig, I. Rungger, G. H. Booth, J. Tennyson, *Phys. Rep.* **2022**, *986*, 1.
- [33] V. E. Elfving, B. W. Broer, M. Webber, J. Gavartin, M. D. Halls, K. P. Lorton, A. Bochevarov (Preprint) arXiv:2009.12472, Submitted: **2020**.
- [34] J. F. Gonthier, M. D. Radin, C. Buda, E. J. Duskocil, C. M. Abuan, J. Romero (Preprint) arXiv:2012.04001, Vol. 7, Submitted: **2020**.
- [35] A. Pellow-Jarman, I. Sinayskiy, A. Pillay, F. Petruccione, *Quantum Inf. Process.* **2021**, *20*, 202.

- [36] G. S. Ravi, P. Gokhale, Y. Ding, W. Kirby, K. Smith, J. M. Baker, P. J. Love, H. Hoffmann, K. R. Brown, F. T. Chong, in *Proc. of the 28th ACM Int. Conf. on Architectural Support for Programming Languages and Operating Systems*, Vancouver BC Canada Vol. 1, **2022**, pp. 15–29.
- [37] D. Wierichs, C. Gogolin, M. Kastoryano, *Phys. Rev. Res.* **2020**, 2, 043246.
- [38] C. Batista, G. Ortiz, *Phys. Rev. Lett.* **2001**, 86, 1082.
- [39] E. Fradkin, *Phys. Rev. Lett.* **1989**, 63, 322.
- [40] V. Galitski, *Phys. Rev. B: Condens. Matter Mater. Phys.* **2010**, 82, 060411.
- [41] G. B. Mbeng, A. Russomanno, G. E. Santoro, *SciPost Phys. Lect. Notes* **2024**, 082. <http://dx.doi.org/10.21468/SciPostPhysLectNotes.82>.
- [42] R. Wiersema, C. Zhou, Y. de Sereville, J. F. Carrasquilla, Y. B. Kim, H. Yuen, *PRX Quantum* **2020**, 1, 020319.
- [43] D. Wecker, M. B. Hastings, M. Troyer, *Phys. Rev. A* **2015**, 92, 042303.